SCIENCE CHINA
Information Sciences

• RESEARCH PAPER •

August 2022, Vol. 65 182205:1–182205:14
https://doi.org/10.1007/s11432-020-3192-5

Estimation and compensation of periodic disturbance using internal-model-based equivalent-input-disturbance approach

Qicheng MEI[1,2], Jinhua SHE[3*], Zhentao LIU[1,2] & Min WU[1,2]

[1]*School of Automation, China University of Geosciences, Wuhan* 430074, *China;*
[2]*Hubei Key Laboratory of Advanced Control and Intelligent Automation for Complex Systems, Wuhan* 430074, *China;*
[3]*School of Engineering, Tokyo University of Technology, Hachioji* 192-0982, *Japan*

Received 27 September 2020/Revised 9 December 2020/Accepted 2 February 2021/Published online 27 July 2022

Abstract This paper presents an improved equivalent-input-disturbance (EID) approach to deal with periodic disturbances. The approach has two degrees of freedom. One is an improved EID compensator, in which a repetitive controller is inserted in this study. The other is a conventional servo system for a reference input. The improved EID compensator estimates and compensates for periodic disturbances without steady-state error, and the servo system ensures a satisfactory tracking performance. The improved EID compensator is designed using the linear-matrix-inequality (LMI) method. Three parameters in an LMI are selected using the particle-swarm-optimization (PSO) algorithm. The state-feedback gain of the conventional servo system is designed using the linear-quadratic-regulator (LQR) method. Simulation results of a rotational control system demonstrate the validity of the approach and its advantage over others.

Keywords equivalent input disturbance (EID), linear matrix inequality (LMI), linear quadratic regulator (LQR), particle swarm optimization (PSO), periodic disturbance, repetitive control

Citation Mei Q C, She J H, Liu Z T, et al. Estimation and compensation of periodic disturbance using internal-model-based equivalent-input-disturbance approach. Sci China Inf Sci, 2022, 65(8): 182205, https://doi.org/10.1007/s11432-020-3192-5

1 Introduction

While tracking a reference input is the main objective in system control, the suppression of disturbances is also important to guarantee control precision. Periodic disturbances, such as the eccentricity of a shaft [1], the cutting force of noncircular cutting systems [2], and harmonics in power systems [3] degrade control performance. The rejection of periodic disturbances is therefore a key to improving control precision and performance [4, 5].

The internal model principle (IMP) [6] reveals that a disturbance is completely rejected in a steady state if a generator of the disturbance is contained in the controller in a system. A repetitive controller is an internal model of a periodic signal with its delay time being exactly the period of the signal. Thus, a repetitive-control system (RCS) ensures the high precision of disturbance rejection for periodic signals, and they have been used extensively in control engineering practice [7].

A control system containing an equivalent-input-disturbance (EID) compensator has been presented to suppress disturbances in a control system [8]. The basic idea of the EID approach is that it takes the effect of disturbances on the output of a plant to be that caused by an artificial disturbance on the control input channel, which is called an EID. An estimate of the EID is used to compensate for the disturbances. It is able to handle both matched and unmatched exogenous disturbances. Notably, an EID-based control system has two degrees of freedom. One is used to guarantee feedback performance and the other is used to estimate and compensate for disturbances. Thus, such a control system has both satisfied feedback and disturbance-rejection performance [9]. The EID approach has been successfully applied to uncertain

* Corresponding author (email: she@stf.teu.ac.jp)

systems [10], time-delay systems [11,12], nonlinear systems [13,14], and fractional-order systems [15]. To further improve the disturbance-rejection performance, a gain matrix was used in an EID compensator to improve the accuracy of the disturbance estimation [16]. An adaptive law was derived to adjust the gain in an EID estimator to maximize the potential of disturbance rejection [17]. A stable zero was added to an EID estimator to compensate for the phase lag caused by a low-pass filter in the estimator [18]. While these studies improved the performance of disturbance estimation from different perspectives, it cannot compensate for disturbances completely in steady state because an EID estimator does not contain an internal model of disturbances.

This paper describes a new EID-based approach in which we extend the EID approach to repetitive control (it is called the RC-EID approach hereafter) to estimate and compensate for periodic disturbances. First, we present the structure of the RC-EID-based control system. Next, we analyze the conventional EID estimator and explain its limitation in the rejection of periodic disturbances. An RC-EID estimator in the system is used to overcome the limitations of the conventional RCS. Then, we investigate the stability and disturbance-rejection mechanism of the system. We design the compensator using a linear matrix inequality (LMI), in which three adjustable parameters are tuned using the particle-swarm-optimization (PSO) algorithm to achieve optimal disturbance-rejection performance. The gain of the state feedback is designed using the linear-quadratic-regulator (LQR) method to guarantee the input tracking performance. Finally, a rotational-speed-control system is used to demonstrate the validity of the method.

In this paper, $\mathbb{R}^n$ is the set of an n-dimensional column vectors, $\mathbb{R}^{n\times n}$ is the set of $n\times n$ real matrices, a symmetric matrix $\left[\begin{smallmatrix} A & B \\ B^{\mathrm{T}} & C \end{smallmatrix}\right]$ is denoted as $\left[\begin{smallmatrix} A & B \\ \star & C \end{smallmatrix}\right]$, and $X(s)$ is the Laplace transform of $x(t)$. For a transfer function matrix $G(j\omega)$, $\|G(j\omega)\|$ is the maximum singular value of $G(j\omega)$ at the angular frequency ω.

2 System configuration and stability analysis

This section first formulates the problem considered in this study. Then, it shows the configuration of the RC-EID-based control system, explains the limitation of the conventional EID approach, and analyzes the stability of the RC-EID-based control system.

2.1 Problem formulation

Consider a single-input single-output plant with a periodic exogenous disturbance:

$$\begin{cases} \dot{x}(t) = Ax(t) + Bu(t) + B_d d(t), \\ y(t) = Cx(t), \end{cases} \tag{1}$$

where $x(t)$ ($\in \mathbb{R}^n$) is the state; $u(t)$ ($\in \mathbb{R}$) is the control input; $y(t)$ ($\in \mathbb{R}$) is the output; $d(t)$ ($\in \mathbb{R}^d$) is a periodic disturbance with the fundamental angular frequency of ω_f; and A ($\in \mathbb{R}^{n\times n}$), B ($\in \mathbb{R}^{n\times 1}$), B_d ($\in \mathbb{R}^{n\times d}$), and C ($\in \mathbb{R}^{1\times n}$) are constant matrices.

As explained in [8], there exists an EID, $d_e(t)$ ($\in \mathbb{R}$), on the control input channel that has the same effect on the output, $y(t)$, as $d(t)$ does. Using $d_e(t)$ to describe the plant (1) gives

$$\begin{cases} \dot{x}(t) = Ax(t) + B[u(t) + d_e(t)], \\ y(t) = Cx(t). \end{cases} \tag{2}$$

The following assumptions are made for the plant.

Assumption 1. The linear system (A, B, C) is controllable and observable.

Assumption 2. Both $d(t)$ and $d_e(t)$ are bounded, that is, there exist positive constants d_M ($<\infty$) and d_{eM} ($<\infty$) such that

$$|d(t)| \leqslant d_M, \quad |d_e(t)| \leqslant d_{eM}, \quad t \in [0,\ \infty).$$

The problems considered in this study involve devising a control system that tracks a step reference input $r(t)$ and rejects the periodic disturbance $d(t)$ that has a period

$$T = 2\pi/\omega_f. \tag{3}$$

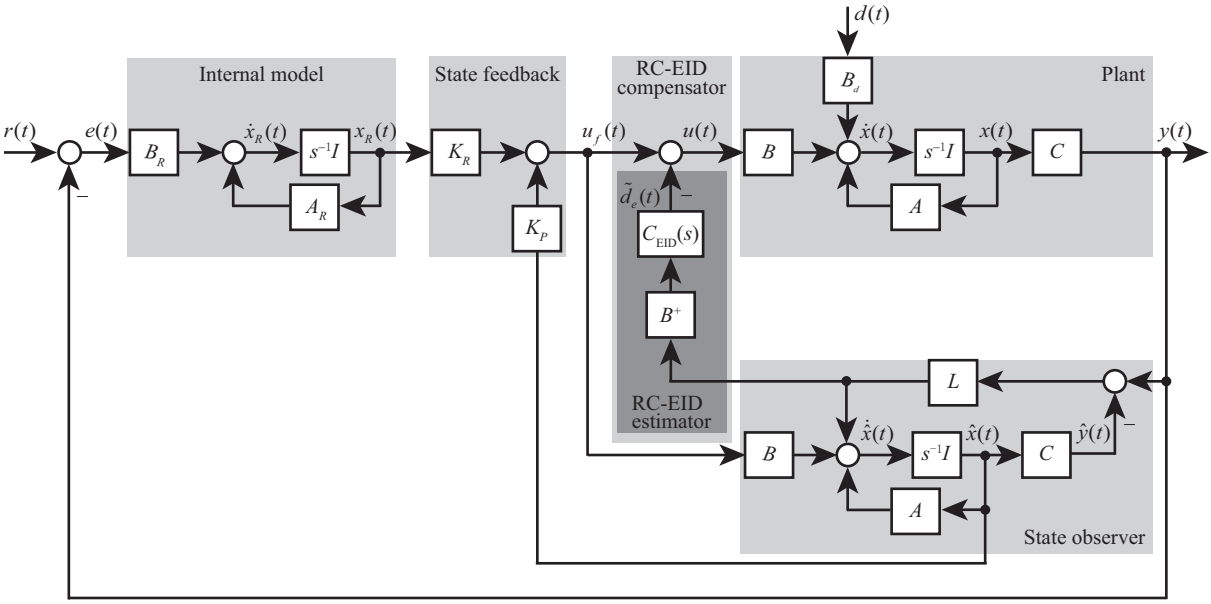

Figure 1 Configuration of RC-EID-based control system.

2.2 Configuration of RC-EID-based control system

The RC-EID-based control system (Figure 1) has five parts: the plant, an internal model, a state-feedback controller, a state observer, and an RC-EID compensator that contains an RC-EID estimator.

An internal model of a step reference $r(t)$ is

$$\dot{x}_R(t) = A_R x_R(t) + B_R[r(t) - y(t)], \tag{4}$$

where $x_R(t)$ ($\in \mathbb{R}$) is the state of the internal model; A_R ($\in \mathbb{R}$) and B_R ($\in \mathbb{R}$) are the system and input matrices, respectively. This model guarantees perfect reference tracking.

The state observer is

$$\begin{cases} \dot{\hat{x}}(t) = A\hat{x}(t) + Bu_f(t) + L[y(t) - \hat{y}(t)], \\ \hat{y}(t) = C\hat{x}(t), \end{cases} \tag{5}$$

where $\hat{x}(t)$ ($\in \mathbb{R}^n$) is the state of the observer, $u_f(t)$ ($\in \mathbb{R}$) is the state feedback input, and L ($\in \mathbb{R}^n$) is the observer gain.

An estimate of $d_e(t)$ is [8]

$$\hat{d}(t) = -B^+ LC\Delta x(t) + u_f(t) - u(t), \tag{6}$$

where

$$B^+ = (B^{\mathrm{T}}B)^{-1}B^{\mathrm{T}}, \tag{7}$$

$$\Delta x(t) = \hat{x}(t) - x(t). \tag{8}$$

A first-order low-pass filter

$$F_e(s) = \frac{1}{T_e s + 1} \tag{9}$$

was used to select an angular-frequency band for disturbance rejection in the conventional EID estimator (Figure 2, [9]). The filtered signal $\tilde{d}(t)$ is given by

$$\tilde{D}(s) = F_e(s)\hat{D}(s). \tag{10}$$

Using (9) to simplify Figure 2 yields Figure 3. Thus,

$$\tilde{D}(s) = -C_{\mathrm{EID}}(s)B^+ LC\Delta X(s),\ C_{\mathrm{EID}}(s) = \frac{1}{T_e}\frac{1}{s}. \tag{11}$$

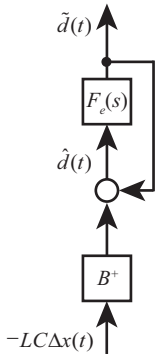

Figure 2 EID estimator.

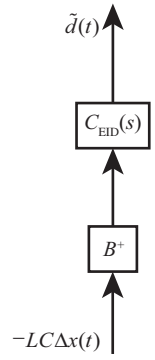

Figure 3 Simplification of Figure 2.

Notably, $C_{\mathrm{EID}}(s)$ in (11) contains $1/s$, which is an internal model of a step signal. Therefore, the conventional EID compensator is able to completely reject a step disturbance in a steady state. However, it cannot completely compensate for periodic disturbances.

In this study, we insert a repetitive controller in $C_{\mathrm{EID}}(s)$ to improve the periodic-disturbance rejection performance:

$$C_{\mathrm{EID}}(s) = \frac{K_q q(s)}{1 - q(s)\mathrm{e}^{-Ts}}, \tag{12}$$

where K_q is the gain and

$$q(s) = \frac{\omega_q}{s + \omega_q} \tag{13}$$

is a first-order low-pass filter. The cutoff angular frequency ω_q is chosen to be

$$\omega_q = (5 \sim 10)\ \omega_r, \tag{14}$$

where ω_r is the highest angular frequency for disturbance estimation and rejection.

As a result, an estimate of $d_e(t)$ is given by

$$\tilde{D}_e(s) = -C_{\mathrm{EID}}(s)B^+LC\Delta X(s). \tag{15}$$

Selecting the delay time in (12) to be the period of $d(t)$ in (3) ensures that $C_{\mathrm{EID}}(s)$ is an internal model of $d(t)$, and $\tilde{d}_e(t)$ converges to $d_e(t)$ for a properly designed $C_{\mathrm{EID}}(s)$.

Incorporating $\tilde{d}_e(t)$ in the control input, which is called an RC-EID compensator, yields the following control law to compensate for $d_e(t)$:

$$u(t) = u_f(t) - \tilde{d}_e(t), \tag{16}$$

where

$$u_f(t) = [K_P \quad K_R] \begin{bmatrix} \hat{x}(t) \\ x_R(t) \end{bmatrix} \tag{17}$$

and $[K_P \quad K_R]$ is the feedback-gain matrix.

Remark 1. While the conventional EID approach estimates and compensates for a disturbance without being aware of the use of the IMP, the RC-EID approach actively makes use of the IMP. This provides us a way to completely compensate for a periodic disturbance. The configuration of the RC-EID-based control system shows a new way of using a high-order EID estimator.

2.3 Analysis of stability and disturbance-rejection mechanism

Combining (2), (5), (8), and (16) yields

$$\Delta\dot{x}(t) = (A - LC)\Delta x(t) + B[\tilde{d}_e(t) - d_e(t)]. \tag{18}$$

Redrawing Figure 1 based on (2), (4), (8), and (15)–(18) yields Figure 4, where

$$u_d(t) = d_e(t) - \tilde{d}_e(t) + K_P\Delta x(t) + K_R x_R(t), \tag{19}$$

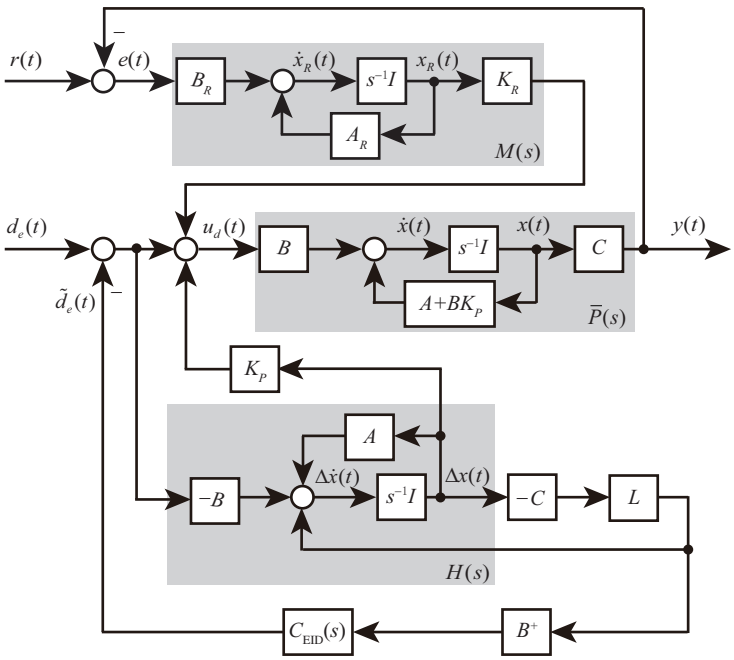

Figure 4 Block diagram from exogenous signals to output.

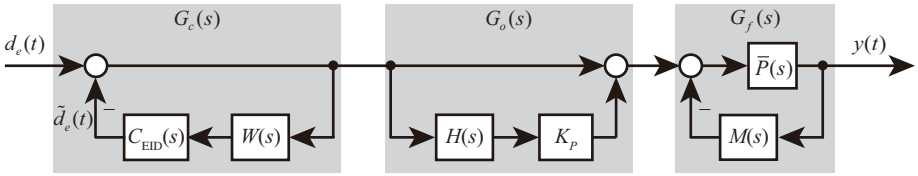

Figure 5 Block diagram from $d_e(t)$ to $y(t)$.

and

$$M(s) = K_R[sI - A_R]^{-1}B_R, \tag{20}$$
$$\bar{P}(s) = C[sI - (A + BK_P)]^{-1}B, \tag{21}$$
$$H(s) = -[sI - (A - LC)]^{-1}B. \tag{22}$$

Letting $r(t) = 0$ and redrawing Figure 4 yield Figure 5, where

$$W(s) = -B^{+}LCH(s), \tag{23}$$
$$G_f(s) = \bar{P}(s)[1 + \bar{P}(s)M(s)]^{-1}, \tag{24}$$
$$G_o(s) = 1 + K_P H(s), \tag{25}$$
$$G_c(s) = [1 + C_{\mathrm{EID}}(s)W(s)]^{-1}. \tag{26}$$

Figure 5 shows that the system contains three subsystems in series: the RC-EID compensator, $G_c(s)$; an observer error system, $G_o(s)$; and the plant with the state feedback, $G_f(s)$. Thus, the stability of the system is guaranteed if all three subsystems are stable [19].

The transfer function from the EID, $d_e(t)$, to the output $y(t)$ is

$$G_{dy}(s) = G_c(s)G_o(s)G_f(s).$$

It is necessary to ensure

$$\|G_c(jk\omega_f)\| \approx 0, \quad k = \pm 1, \pm 2, \ldots \tag{27}$$

to reject the periodic disturbance.

For the system in Figure 5, let

$$\varepsilon = \left\| [C_{\mathrm{EID}}(jk\omega_f)W(jk\omega_f)]^{-1} \right\|. \tag{28}$$

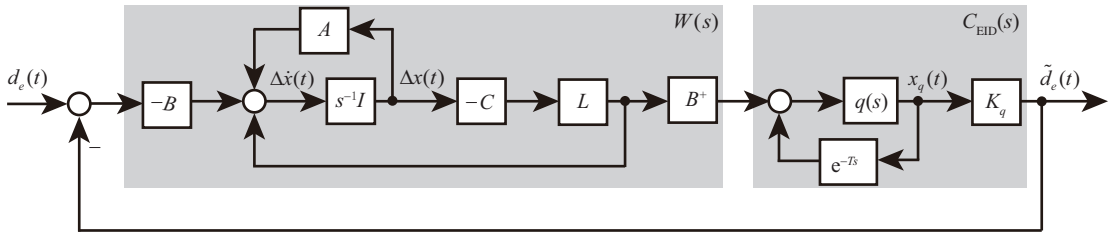

Figure 6 Block diagram from $d_e(t)$ to $\tilde{d}_e(t)$.

We choose K_q such that

$$\varepsilon \ll 1 \tag{29}$$

holds. Thus,

$$\|C_{\mathrm{EID}}(jk\omega_f)W(jk\omega_f)\| \gg 1 \tag{30}$$

is true. Eq. (26) and Inequality (30) ensure that Eq. (27) holds, that is, $\tilde{d}_e(t)$ is a good estimate of $d_e(t)$ in both transient response and a steady state. As a result, the control law (16) rejects the disturbance.

3 Design of RC-EID-based control system

This section explains the design of the repetitive controller, the state observer, and the feedback gains of the RC-EID-based control system to meet the requirements of stability and disturbance rejection.

3.1 Design of state observer and repetitive controller

Let the singular-value decomposition of a matrix Π ($\in \mathbb{R}^{p\times m}$) be

$$\Pi = \bar{U}\begin{bmatrix}\bar{S} & 0\end{bmatrix}\bar{V}^{\mathrm{T}}, \tag{31}$$

where $\bar{S}$ ($\in \mathbb{R}^{m\times m}$) is a positive-definite matrix, and $\bar{U}$ ($\in \mathbb{R}^{m\times m}$) and $\bar{V}$ ($\in \mathbb{R}^{p\times p}$) are unitary matrices.

The following lemmas are employed for the derivation of the stability condition of the RC-EID compensator, $G_c(s)$.

Lemma 1 ([20])**.** For a given matrix $\Pi \in \mathbb{R}^{p\times m}$ with $\mathrm{rank}(\Pi) = p$, there exists a matrix $\bar{X} \in \mathbb{R}^{p\times p}$ such that

$$\Pi X = \bar{X}\Pi$$

holds for any $X \in \mathbb{R}^{m\times m}$ if and only if X can be decomposed as

$$X = \bar{V}\begin{bmatrix}\bar{X}_{11} & 0\\ 0 & \bar{X}_{22}\end{bmatrix}\bar{V}^{\mathrm{T}}, \tag{32}$$

where $\bar{V} \in \mathbb{R}^{m\times m}$ is a unitary matrix, $\bar{X}_{11} \in \mathbb{R}^{p\times p}$, and $\bar{X}_{22} \in \mathbb{R}^{(m-p)\times(m-p)}$.

Lemma 2 (Schur complement, [21])**.** For a given symmetric matrix

$$\chi = \begin{bmatrix}\chi_{11} & \chi_{12}\\ \star & \chi_{22}\end{bmatrix},$$

the following statements are equivalent:

(1) $\chi < 0$;

(2) $\chi_{11} < 0$ and $\chi_{22} - \chi_{12}^{\mathrm{T}}\chi_{11}^{-1}\chi_{12} < 0$; and

(3) $\chi_{22} < 0$ and $\chi_{11} - \chi_{12}\chi_{22}^{-1}\chi_{12}^{\mathrm{T}} < 0$.

The stability condition for the system from $d_e(t)$ to $\tilde{d}_e(t)$ (Figure 6) is the same as that for the compensator, $G_c(s)$. The state equation of $C_{\mathrm{EID}}(s)$ is

$$\dot{x}_q(t) = -\omega_q x_q(t) + \omega_q x_q(t-T) - \omega_q B^{+}LC\Delta x(t). \tag{33}$$

And that of $W(s)$ is

$$\Delta\dot{x}(t) = (A - LC)\Delta x(t) + K_q B x_q(t) - B d_e(t). \tag{34}$$

Let $\tilde{x}(t) = [x_q(t) \;\; \Delta x^{\mathrm{T}}(t)]^{\mathrm{T}}$. Then, the closed-loop system of Figure 6 is

$$\dot{\tilde{x}}(t) = \tilde{A}x(t) + \tilde{A}_d x(t-T) + \tilde{B}d_e(t), \tag{35}$$

where

$$\tilde{A} = \begin{bmatrix} -\omega_q & -\omega_q B^{+} LC \\ K_q B & A - LC \end{bmatrix}, \quad \tilde{A}_d = \begin{bmatrix} \omega_q & 0 \\ 0 & 0 \end{bmatrix}, \quad \tilde{B} = \begin{bmatrix} 0 \\ -B \end{bmatrix}.$$

Assume that the singular-value decomposition of the output matrix is

$$C = U[\hat{S} \;\; 0]\hat{V}^{\mathrm{T}}, \tag{36}$$

where $\hat{S}$ is a semi-positive definite matrix, U and $\hat{V}^{\mathrm{T}}$ are unitary matrices. Let $\hat{V}$ be

$$\hat{V} = [\hat{V}_1 \;\; \hat{V}_2], \tag{37}$$

and then the stability of the system (35) is given by the following theorem.

Theorem 1. For a given cutoff angular frequency ω_q and positive scalars α, β, and γ, if there exist symmetric positive-definite matrices X_1, X_2, Y_1, and Y_2, and appropriate matrices M_1 and M_2, such that the following LMI holds:

$$\begin{bmatrix} \Psi_{11} & \Psi_{12} & \omega_q Y_1 & 0 & X_1 & 0 & 0 \\ \star & \Psi_{22} & 0 & 0 & 0 & X_2 & -B \\ \star & \star & -Y_1 & 0 & 0 & 0 & 0 \\ \star & \star & \star & -Y_2 & 0 & 0 & 0 \\ \star & \star & \star & \star & -Y_1 & 0 & 0 \\ \star & \star & \star & \star & \star & -Y_2 & 0 \\ \star & \star & \star & \star & \star & \star & -\gamma^2 I \end{bmatrix} < 0, \tag{38}$$

where

$$\begin{aligned} \Psi_{11} &= -2\alpha^2 \omega_q X_1, \\ \Psi_{12} &= \alpha\beta\left(-\omega_q B^{+} M_2 C + M_1^{\mathrm{T}} B^{\mathrm{T}}\right), \\ \Psi_{22} &= \beta^2\left[(AX_2 - M_2 C) + (AX_2 - M_2 C)^{\mathrm{T}}\right], \end{aligned}$$

then the system (35) is asymptotically stable. Moreover, if the singular-value decomposition of X_2 is

$$X_2 = \begin{bmatrix} \hat{V}_1 & \hat{V}_2 \end{bmatrix} \begin{bmatrix} X_{21} & 0 \\ 0 & X_{22} \end{bmatrix} \begin{bmatrix} \hat{V}_1^{\mathrm{T}} \\ \hat{V}_2^{\mathrm{T}} \end{bmatrix},$$

then the gains K_q and L are given by

$$K_q = M_1 X_1^{-1}, \quad L = M_2 U \hat{S} X_{21}^{-1} \hat{S}^{-1} U^{\mathrm{T}}. \tag{39}$$

Proof. Consider a Lyapunov function candidate

$$V(t) = \tilde{x}^{\mathrm{T}}(t) P \tilde{x}(t) + \int_{t-T}^{t} \tilde{x}^{\mathrm{T}}(\tau) Q \tilde{x}(\tau) \mathrm{d}\tau, \tag{40}$$

where

$$P = \mathrm{diag}\left\{\frac{1}{\alpha} P_1, \; \frac{1}{\beta} P_2\right\}, \quad Q = \mathrm{diag}\left\{Q_1, \; Q_2\right\}.$$

First, let

$$P_1 = X_1^{-1}, \quad P_2 = X_2^{-1}, \quad Q_1 = Y_1^{-1}, \quad Q_2 = Y_2^{-1}.$$

Calculating the derivative of $V(t)$ along the system (35) yields

$$\dot{V}(t) = \varphi^{\mathrm{T}}(t)\Phi_0\varphi(t) + 2\tilde{x}^{\mathrm{T}}(t)P\tilde{B}d_e(t), \tag{41}$$

where

$$\varphi(t) = \begin{bmatrix} \tilde{x}(t) \\ \tilde{x}(t-T) \end{bmatrix}, \quad \Phi_0 = \begin{bmatrix} \tilde{A}^{\mathrm{T}}P + P\tilde{A} + Q & P\tilde{A}_d \\ \star & -Q \end{bmatrix}.$$

Since

$$2\tilde{x}^{\mathrm{T}}(t)P\tilde{B}d_e(t) \leqslant \tilde{x}^{\mathrm{T}}(t)P\tilde{B}\tilde{B}^{\mathrm{T}}P\tilde{x}(t) + d_e^{\mathrm{T}}(t)d_e(t),$$

we have

$$\dot{V}(t) \leqslant \varphi^{\mathrm{T}}(t)\Phi_1\varphi(t) + d_e^{\mathrm{T}}(t)d_e(t), \tag{42}$$

where

$$\Phi_1 = \begin{bmatrix} \tilde{A}^{\mathrm{T}}P + P\tilde{A} + P\tilde{B}\tilde{B}^{\mathrm{T}}P + Q & P\tilde{A}_d \\ \star & -Q \end{bmatrix}.$$

According to Assumption 2, $d_e(t)$ is bounded. If $\Phi_1 < 0$ holds, then the system (35) is asymptotically stable [22]. From Lemma 2, it is clear that $\Phi_1 < 0$ is equivalent to

$$\begin{bmatrix} \tilde{A}^{\mathrm{T}}P + P\tilde{A} & P\tilde{A}_d & Q & P\tilde{B} \\ \star & -Q & 0 & 0 \\ \star & \star & -Q & 0 \\ \star & \star & \star & -I \end{bmatrix} < 0. \tag{43}$$

Next, applying Lemma 1 to the output matrix C gives

$$CX_2 = \bar{X}_2 C. \tag{44}$$

Then, letting

$$X_2 = \begin{bmatrix} \hat{V}_1 & \hat{V}_2 \end{bmatrix} \begin{bmatrix} X_{21} & 0 \\ 0 & X_{22} \end{bmatrix} \begin{bmatrix} \hat{V}_1^{\mathrm{T}} \\ \hat{V}_2^{\mathrm{T}} \end{bmatrix}, \quad K_q X_1 = M_1, \quad L\bar{X}_2 = M_2 \tag{45}$$

yields

$$\bar{X}_2 = U\hat{S}X_{21}^{-1}\hat{S}^{-1}U^{\mathrm{T}}. \tag{46}$$

Pre- and post-multiplying (43) by $\mathrm{diag}\{\alpha X_1,\ \beta X_2,\ Y_1,\ Y_2,\ Y_1,\ Y_2,\ \gamma I\}$ and combining it with (44)–(46) yield (38) and (39).

Remark 2. The parameters α, β, and γ are used to adjust the control performance. More specifically, α is mainly for K_q, β for L, and γ for H_∞.

3.2 Parameter optimization

Among feasible solutions to LMI (38), we find one that achieves the best disturbance-rejection performance. Therefore, a PSO algorithm (Figure 7) is used to find the best combination of α, β, and γ in Theorems 1.

We choose a fitness function

$$J = \left| \frac{1}{\varepsilon} - m \right| \tag{47}$$

to evaluate the particles for the PSO algorithm. In (47), ε is given in (28) and m (> 0) is a tuning parameter. A small J means that

$$\varepsilon \approx \frac{1}{m}.$$

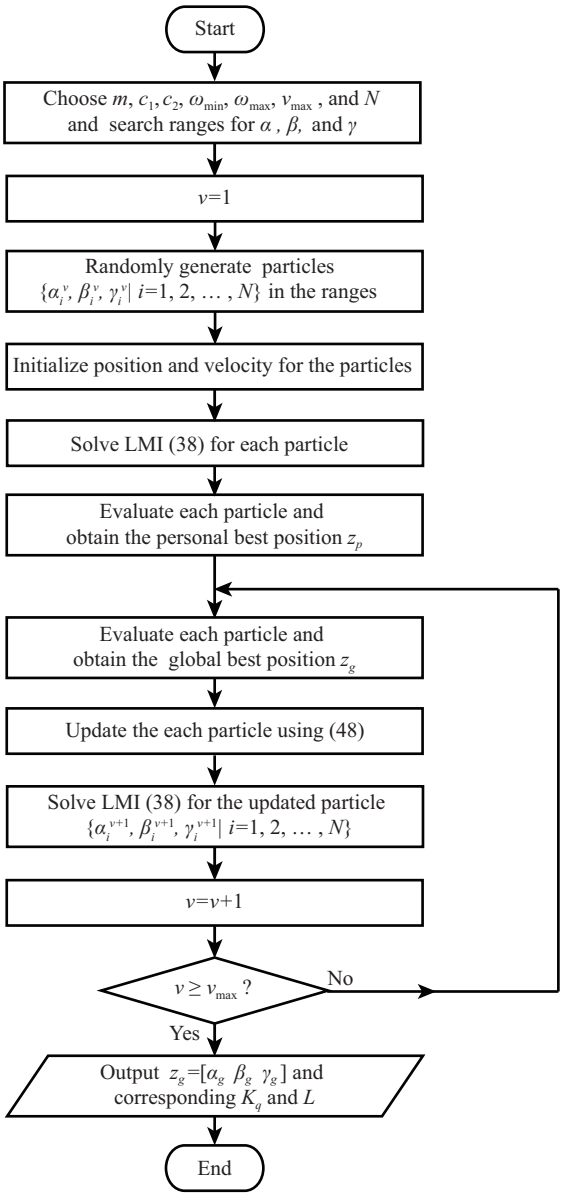

Figure 7 Flowchart of PSO algorithm.

Clearly, a large m results in a small ε. Thus, as explained in Subsection 3.2, it yields a satisfactory disturbance-rejection performance.

The updating laws for the velocity and position of the PSO are

$$\begin{cases} v_i^{(\nu+1)} = wv_i^{(\nu)} + c_1(z_p^{(\nu)} - z_i^{(\nu)}) + c_2(z_g^{(\nu)} - z_i^{(\nu)}), \\ z_i^{(\nu+1)} = z_i^{(\nu)} + v_i^{(\nu+1)}, \end{cases} \tag{48}$$

where $z_i = [\alpha_i \ \beta_i \ \gamma_i]$ and $v_i = [v_{\alpha i} \ v_{\beta i} \ v_{\gamma i}]$ $(i = 1, 2, \dots, N)$ are the current position and velocity, respectively, N is the population size, ν is the number of iterations, z_p is the personal best position, z_g is the global best position, c_1 and c_2 are acceleration constants, and w is the inertia weight. To balance the global search velocity and the local search accuracy, w is updated by

$$w = w_{\max} - (w_{\max} - w_{\min})\frac{\nu}{\nu_{\max}}, \tag{49}$$

where $w_{\max}$ and $w_{\min}$ are the maximum and minimum weights, respectively; $\nu_{\max}$ is the maximum iteration number.

Remark 3. The use of the frequency-domain performance index J in (47) significantly reduces the computational complexity of the PSO algorithm because it avoids the integral operation of the tracking error $e(t)$ in a time-domain performance index.

3.3 Design of state-feedback gains

Redrawing Figure 4 yields Figure 8. The Laplace transform of the tracking error $e(t)$ is

$$E(s) = \frac{1}{1 + M(s)\bar{P}(s)} R(s) + \frac{G_c(s)G_o(s)\bar{P}(s)}{1 + M(s)\bar{P}(s)} D_e(s). \tag{50}$$

The exogenous disturbance is rejected by the compensator $G_c(s)$, and the internal model $M(s)$ is used to guarantee the input-tracking performance.

A state-space model containing the plant and the internal model of a step signal is

$$\dot{\bar{x}}(t) = \bar{A}\bar{x}(t) + \bar{B}\bar{u}(t) + \bar{B}_R r(t), \tag{51}$$

where $\bar{x}(t) = [x^{\mathrm{T}}(t) \;\; x_R^{\mathrm{T}}(t)]^{\mathrm{T}}$, and

$$\bar{A} = \begin{bmatrix} A & 0 \\ -B_R C & A_R \end{bmatrix}, \quad \bar{B} = \begin{bmatrix} B \\ 0 \end{bmatrix}, \quad \bar{B}_R = \begin{bmatrix} 0 \\ B_R \end{bmatrix}.$$

The state-feedback control law is

$$u = \bar{K}\bar{x}(t), \quad \bar{K} = [K_P \;\; K_R]. \tag{52}$$

Minimizing the performance index

$$J_K = \int_0^\infty \left\{ \bar{x}^{\mathrm{T}}(t) Q_K \bar{x}(t) + u^{\mathrm{T}}(t) R_K u(t) \right\} \mathrm{d}t \tag{53}$$

yields

$$[K_P \; K_R] = -R_K^{-1} \bar{B}^{\mathrm{T}} P, \tag{54}$$

where P is the solution of a Riccati equation,

$$\bar{A}^{\mathrm{T}} P + P\bar{A} - P\bar{B} R_K^{-1} \bar{B}^{\mathrm{T}} P + Q_K = 0.$$

Remark 4. Notably, the input-tracking performance depends on K_P and K_R, which can be adjusted by Q_K and R_K. This means that the RC-EID approach overcomes the limitations of the conventional RCS.

3.4 Design procedure

Extracting the key points from the above discussion gives the following design steps for the RC-EID-based control system:

Step 1. Choose the delay time T for the repetitive controller $C_{\mathrm{EID}}(s)$.

Step 2. Choose the highest angular frequency ω_r for the disturbance estimation and rejection.

Step 3. Choose the low-pass filter in the repetitive controller that satisfies

$$q(j\omega) \approx 1, \quad \omega \in [0, \; \omega_r]. \tag{55}$$

Step 4. Design the gain in repetitive controller K_q and the state observer gain L by optimizing (47).

Step 5. Check if $H(s)$ (that is, $G_o(s)$) is stable. If it is not, return to Step 4 and redesign K_q and L. Otherwise, continue.

Step 6. Design the feedback gains, K_P and K_R, by optimizing (53).

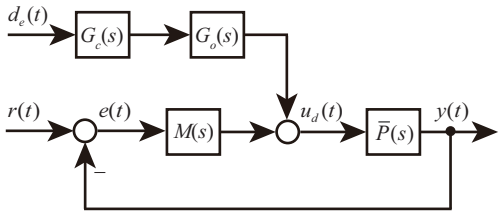

Figure 8 Simplification of Figure 4.

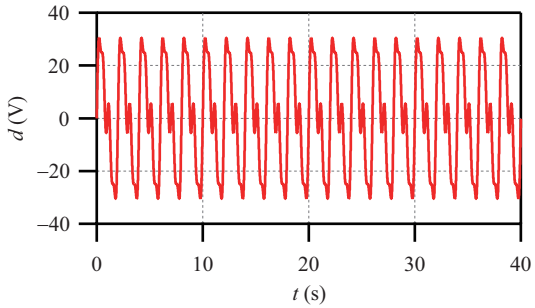

Figure 9 (Color online) Periodic disturbance.

4 Simulation verification

Consider a rotational control system with the parameters of the plant (1) being the same as those in [8]:

$$A=\begin{bmatrix}-31.31 & 0 & -28330\\ 0 & -10.25 & 8001\\ 1 & -1 & 0\end{bmatrix},\ B=\begin{bmatrix}28.06\\ 0\\ 0\end{bmatrix},\ B_d=\begin{bmatrix}0\\ 7.210\\ 0\end{bmatrix},\ C=\begin{bmatrix}1 & 0 & 0\end{bmatrix}. \tag{56}$$

The following disturbance (Figure 9)

$$d(t)=25\sin\pi t+12.5\sin 2\pi t+6.25\sin 4\pi t \tag{57}$$

was added to the plant. A simple verification shows that this system satisfies Assumptions 1 and 2.

First, since $\omega_f=\pi$ rad/s and $\omega_r=4\pi$ rad/s, we select $T=2$ s and $\omega_q=100$ rad/s.

Next, we choose the parameters of the PSO algorithm to be

$$c_1=1,\quad c_2=1,\quad w_{\max}=1.2,\quad w_{\min}=0.4,\quad \nu_{\max}=100,\quad N=100,\quad m=1000$$

and the search ranges to be

$$\begin{cases} v_i\in[-10,\ 10],\\ \alpha\in(0,\ 500],\ \beta\in(0,\ 500],\ \gamma\in(0,\ 500].\end{cases}$$

The PSO algorithm yields

$$\begin{cases} J=0.0211,\\ \alpha_g=37.8587,\ \beta_g=201.4861,\ \gamma_g=164.8168\end{cases} \tag{58}$$

and

$$\begin{cases} K_q=-1141.0737,\\ L=[-31.3051\ \ -60.5391\ \ -4.9862]^{\mathrm{T}}.\end{cases} \tag{59}$$

The relationship between the fitness and population size is shown in Figure 10.

For a reference input

$$r(t)=1\times 1000(t)\ \text{rpm}, \tag{60}$$

we choose the internal model to be

$$A_R=0,\quad B_R=1.$$

Choosing

$$Q_K=\mathrm{diag}\{1,\ 1,\ 1,\ 10\},\quad R_K=1$$

in (53) yields

$$K_P=[0.4222\ \ 0.1394\ \ -1.4717],\quad K_R=-3.1623. \tag{61}$$

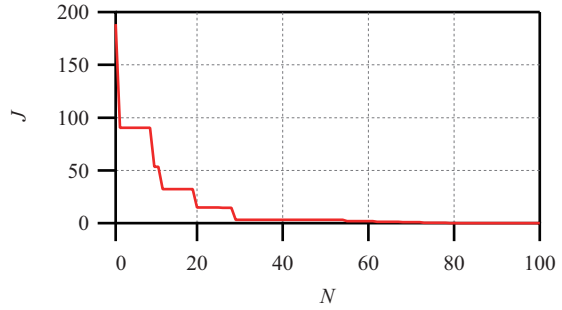

Figure 10 (Color online) Relationship between fitness and population size.

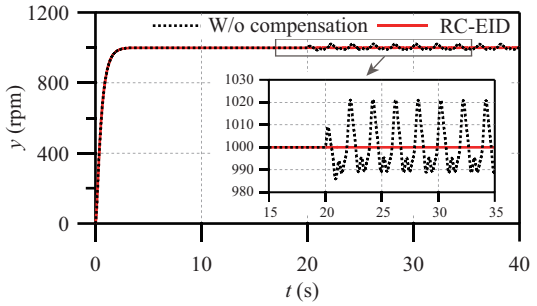

Figure 11 (Color online) Time response of RC-EID approach.

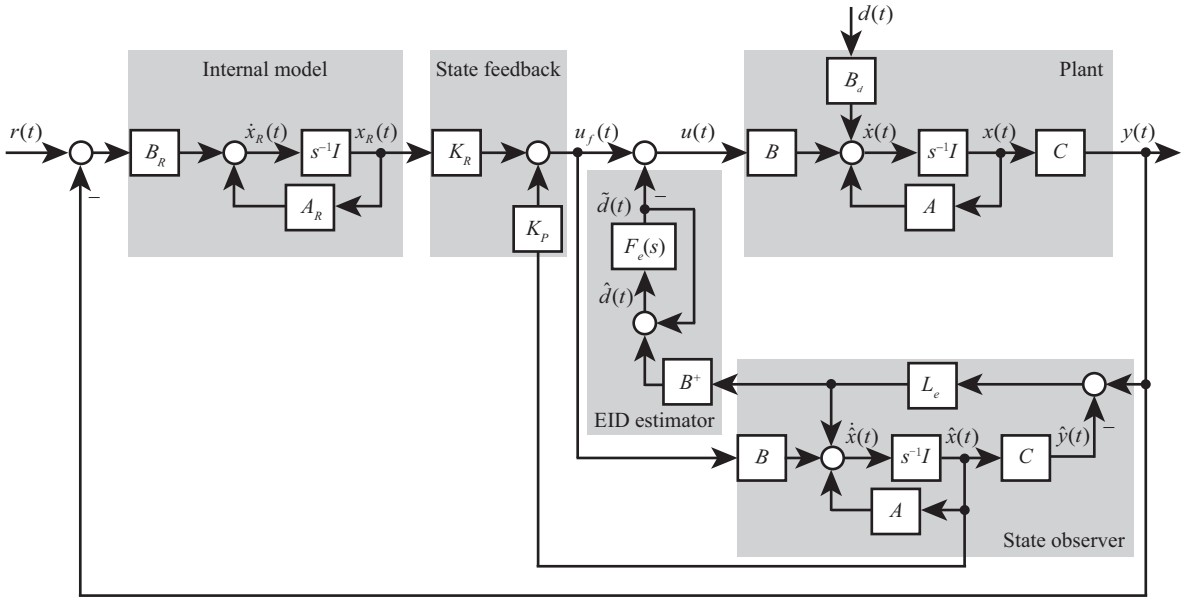

Figure 12 Configuration of EID-based control system.

Simulation results are shown in Figure 11. The step reference input is imposed at $t = 0$ s. After the system enters the steady state, the disturbance is imposed on the system at $t = 20$ s. The peak-to-peak value of the RC-EID approach is less than 0.0941 rpm, which is 0.27% of the method without the RC-EID compensator (35.1822 rpm).

To demonstrate the advantage of the RC-EID approach, we compare the RC-EID approach with the conventional EID approach (Figure 12). The differences between the two approaches are the EID compensator, which contains the filter and the observer gain. The filter in the conventional EID approach is designed to be

$$F_e(s) = \frac{1}{0.01s + 1}.$$

Using the concept of perfect regulation as stated in [8] yields the observer gain:

$$L_e = [972.3130 \quad -11.5790 \quad -0.1108]^{\mathrm{T}}. \tag{62}$$

Other parameters (A_R, B_R, K_R, and K_P) are the same as those for the RC-EID approach.

The Bode magnitude plot from the EID to the output (Figure 13) shows that the magnitude is smaller for the RC-EID approach than for the EID approach, especially at the fundamental and harmonic frequencies of the disturbance. Thus, it yields a better periodic-disturbance rejection performance than the EID approach (Figure 14). The peak-to-peak value of the RC-EID approach is 4.68% of the EID approach (1.6476 rpm). Moreover, there is no steady-state error for the RC-EID approach.

We also compare the RC-EID approach with the conventional RCS (Figure 15), where the repetitive controller $C_R(s)$ is set to be $C_{\mathrm{EID}}(s)$ in (12). For K_P in (61), we set $K_q = 1140$, which ensures that

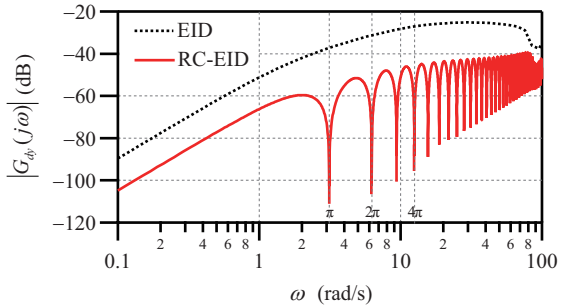

Figure 13 (Color online) Bode magnitude plot from EID to output.

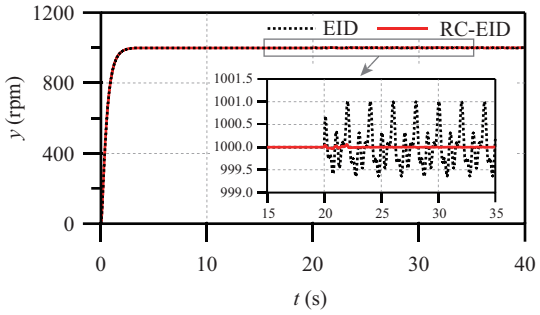

Figure 14 (Color online) Time responses of conventional EID and RC-EID approaches.

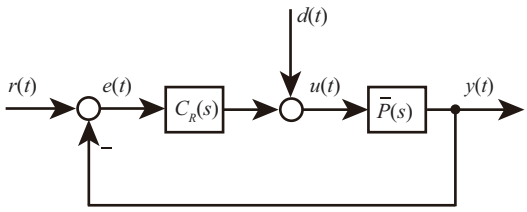

Figure 15 Conventional RCS.

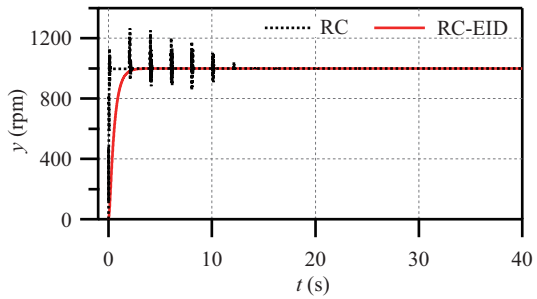

Figure 16 (Color online) Time responses of repetitive control and RC-EID approaches.

the repetitive-control method has the same disturbance-rejection performance as the RC-EID approach. The results are shown in Figure 16. Although they have the same steady-state control performance, the transient performance is better for the RC-EID approach than for the repetitive-control method.

5 Conclusion

This paper presented the RC-EID approach that rejects periodic disturbances and tracks the step reference input. Since the RC-EID estimator contains a repetitive controller, it ensures that a periodic disturbance is rejected without steady-state error. The gains of the repetitive controller and the state observer were designed with the aid of an LMI. A PSO algorithm was used to optimize the disturbance-rejection performance based on a frequency domain performance index, which reduced the computational complexity. A speed control system showed the effectiveness of the RC-EID approach and its advantages over the conventional EID approach. This approach has the following advantages.

(1) The configuration of the RC-EID based control system is simple. It plugs a disturbance compensator into a standard feedback control system.

(2) The RC-EID approach overcomes the limitation of the conventional EID approach by making use of the internal model of a disturbance in an EID estimator to guarantee the steady-state disturbance-rejection performance.

(3) Compared with the conventional repetitive-control method, the RC-EID approach has a satisfactory transient response for a step reference input.

It should be noted that this study focused primarily on linear systems. However, many control systems are nonlinear. Thus, it is important to extend the RC-EID approach to deal with nonlinearities and reject periodic disturbances, and this will be carried out in the future.

Acknowledgements This work was supported in part by National Key R&D Program of China (Grant No. 2017YFB1300900), National Natural Science Foundation of China (Grant No. 61873348), Natural Science Foundation of Hubei Province, China, (Grant No. 2020CFA031), Wuhan Applied Foundational Frontier Project (Grant No. 2020010601012175), and the 111 Project (Grant No. B17040).

References

1 Lu Y S, Lin S M. Disturbance-observer-based adaptive feedforward cancellation of torque ripples in harmonic drive systems. Electr Eng, 2007, 90: 95–106
2 Mei C, Cherng J G, Wang Y. Active control of regenerative chatter during metal cutting process. J Manuf Sci Eng, 2006, 128: 346–349
3 Rech C, Pinheiro H, Grundling H A, et al. Comparison of digital control techniques with repetitive integral action for low cost PWM inverters. IEEE Trans Power Electron, 2003, 18: 401–410
4 Li C Y, Zhang D C, Zhuang X Y. A survey of repetitive control. In: Proceedings of IEEE/RSJ International Conference on Intelligent Robots and Systems, 2004. 1160–1166
5 Ma H, Li H Y, Lu R Q, et al. Adaptive event-triggered control for a class of nonlinear systems with periodic disturbances. Sci China Inf Sci, 2020, 63: 150212
6 Francis B A, Wonham W M. The internal model principle for linear multivariable regulators. Appl Math Optim, 1975, 2: 170–194
7 He J, Luo G Y, Chen J Q. Overview of repetitive control system. Appl Mech Mater, 2014, 536–537: 1174–1177
8 She J H, Fang M X, Ohyama Y, et al. Improving disturbance-rejection performance based on an equivalent-input-disturbance approach. IEEE Trans Ind Electron, 2008, 55: 380–389
9 She J H, Xin X, Pan Y D. Equivalent-input-disturbance approach-analysis and application to disturbance rejection in dual-stage feed drive control system. IEEE/ASME Trans Mechatron, 2011, 16: 330–340
10 Yu P, Wu M, She J H, et al. Robust tracking and disturbance rejection for linear uncertain system with unknown state delay and disturbance. IEEE/ASME Trans Mechatron, 2018, 23: 1445–1455
11 Liu R J, Liu G P, Wu M, et al. Disturbance rejection for time-delay systems based on the equivalent-input-disturbance approach. J Franklin Institute, 2014, 351: 3364–3377
12 Gao F, Wu M, She J H, et al. Delay-dependent guaranteed-cost control based on combination of Smith predictor and equivalent-input-disturbance approach. ISA Trans, 2016, 62: 215–221
13 Ouyang L Y, Wu M, She J H. Estimation of and compensation for unknown input nonlinearities using equivalent-input-disturbance approach. Nonlin Dyn, 2017, 88: 2161–2170
14 Yin X, She J H, Wu M, et al. Disturbance rejection and performance analysis for nonlinear systems based on nonlinear equivalent-input-disturbance approach. Nonlin Dyn, 2020, 100: 3497–3511
15 Liu R J, She J H, Wu M, et al. Robust disturbance rejection for a fractional-order system based on equivalent-input-disturbance approach. Sci China Inf Sci, 2018, 61: 070222
16 Yu P, Wu M, She J H, et al. An improved equivalent-input-disturbance approach for repetitive control system with state delay and disturbance. IEEE Trans Ind Electron, 2018, 65: 521–531
17 Wang Z W, She J H, Wang G J. Adaptive equivalent-input-disturbance approach to improving disturbance-rejection performance. Int J Autom Comput, 2020, 17: 701–712
18 Du Y W, Cao W H, She J H, et al. Disturbance rejection and control system design using improved equivalent input disturbance approach. IEEE Trans Ind Electron, 2020, 67: 3013–3023
19 Anderson B D O, Moore J B. Optimal Control—Linear Quadratic Methods. Englewood Cliffs: Prentice-Hall, 1989
20 Ho D W C, Lu G P. Robust stabilization for a class of discrete-time non-linear systems via output feedback: the unified LMI approach. Int J Control, 2003, 76: 105–115
21 Khargonekar P P, Petersen I R, Zhou K. Robust stabilization of uncertain linear systems: quadratic stabilizability and H_∞ control theory. IEEE Trans Automat Contr, 1990, 35: 356–361
22 Gao Z Q. Active disturbance rejection control: a paradigm shift in feedback control system design. In: Proceedings of the 2006 American Control Conference, Minneapolis, 2006. 2399–2405